HHS Public Access

Author manuscript

Mol Oral Microbiol. Author manuscript; available in PMC 2023 October 01.

Published in final edited form as:

Mol Oral Microbiol. 2022 October ; 37(5): 218–228. doi:10.1111/omi.12379.

Farnesol Delivery *via* Polymeric Nanoparticle Carriers Inhibits Cariogenic Cross-Kingdom Biofilms and Prevents Enamel Demineralization

Tatsuro Ito[1,2,3], **Kenneth R. Sims Jr.**[4], **Yuan Liu**[2,3], **Zhenting Xiang**[2,3], **Rodrigo A. Arthur**[5], **Anderson T. Hara**[6], **Hyun Koo**[2,3], **Danielle S. W. Benoit**[7], **Marlise I. Klein**[8,*]

[1]Department of Pediatric Dentistry, Nihon University School of Dentistry at Matsudo, Chiba, Japan.

[2]Biofilm Research Labs, Levy Center for Oral Health, School of Dental Medicine, University of Pennsylvania, Philadelphia, PA, USA.

[3]Department of Orthodontics and Divisions of Pediatric Dentistry & Community Oral Health, School of Dental Medicine, University of Pennsylvania, Philadelphia, PA, USA.

[4]Department of Translational Biomedical Sciences, University of Rochester School of Medicine and Dentistry, Rochester, NY, USA.

[5]Preventive and Community Dentistry Department, Dental School, Federal University of Rio Grande do Sul, Porto Alegre, Rio Grande do Sul, Brazil.

[6]Department of Cariology, Operative Dentistry and Dental Public Health, Oral Health Research Institute, Indiana University School of Dentistry, Indianapolis, IN, USA.

[7]Department of Biomedical Engineering, Department of Chemical Engineering, Materials Science Program, University of Rochester, Rochester, NY, USA.

[8]Department of Dental Materials and Prosthodontics, São Paulo State University (UNESP), School of Dentistry, Araraquara, São Paulo, Brazil.

Summary

Introduction: *Streptococcus mutans* and *Candida albicans* are frequently detected together in the plaque from patients with early childhood caries (ECC) and synergistically interact to form a cariogenic cross-kingdom biofilm. However, this biofilm is difficult to control. Thus, to achieve maximal efficacy within the complex biofilm microenvironment, nanoparticle carriers have shown increased interest in treating oral biofilms in recent years.

[*]**Corresponding Author:** Marlise I. Klein, Department of Dental Materials and Prosthodontics, São Paulo State University (Unesp), School of Dentistry, Araraquara, Rua Humaitá, 1680, Araraquara, São Paulo 14801-903, Brazil, marlise.klein@unesp.br.

Author Contributions

Ito T, Koo H, Benoit DSW, and Klein MI conceptualized and designed the study. Ito T, Sims K, Liu Y, Xiang Z, Arthur RA, and Hara AT performed the experiments and acquired the data. Ito T, Sims K, Liu Y, Xiang Z, Arthur RA, Hara AT, Koo H, Benoit DSW, and Klein MI analyzed and interpreted the data. Ito T drafted the manuscript. Ito T Sims K, Koo H, Benoit DSW, and Klein MI critically revised the manuscript. All authors contributed to the manuscript and approved the submitted version.

Conflict of interest

The authors declare that the research was conducted in the absence of any commercial or financial relationships that could be construed as a potential conflict of interest.

Methods: Here, we assessed the anti-biofilm efficacy of farnesol (Far), a hydrophobic antibacterial drug and repressor of *Candida* filamentous forms, against cross-kingdom biofilms employing drug delivery *via* polymeric nanoparticle carriers (NPCs). We also evaluated the effect of the strategy on teeth enamel demineralization.

Results: The farnesol-loaded NPCs (NPC+Far) resulted in a 2-log CFU/mL reduction of *S. mutans* and *C. albicans* (hydroxyapatite disc biofilm model). High-resolution confocal images further confirmed a significant reduction in exopolysaccharides, smaller microcolonies of *S. mutans*, and no hyphal form of *C. albicans* after treatment with NPC+Far on human tooth enamel (HT) slabs, altering the biofilm 3D structure. Furthermore, NPC+Far treatment was highly effective in preventing enamel demineralization on HT, reducing lesion depth (79% reduction) and mineral loss (85% reduction) *versus* vehicle PBS-treated HT, while NPC or Far alone had no differences with the PBS.

Conclusion: The drug delivery *via* polymeric NPCs has the potential for targeting bacterial-fungal biofilms associated with a prevalent and costly pediatric oral disease, such as ECC.

Keywords

Nanoparticle carriers; Cross-Kingdom biofilm; Dental caries; Demineralization; Farnesol

Introduction

Streptococcus mutans and *Candida albicans* coinfection is associated with enhanced virulence of dental caries, particularly in early childhood caries (ECC) [Hajishengallis et al., 2017]. The fungus *C. albicans* is frequently detected along with high numbers of *S. mutans* in the plaque of ECC patients, whereas *C. albicans* is either absent or detected sporadically in healthy, caries-free children [de Carvalho et al., 2006; Raja et al., 2010; Yang et al., 2012]. The mannans within the *C. albicans* cell wall provide binding sites for coexistence with *S. mutans*. Moreover, *C. albicans* upregulates *S. mutans*-derived exoenzymes, glucosyltransferase B (GtfB), and accelerates exopolysaccharides (EPS) production, synergistically enhancing the microbial carriage and aciduric activities [Koo et al., 2018]. Notably, *S. mutans* coexisting with *C. albicans* grows more rapidly and forms larger microcolonies than *S. mutans* alone [Kim et al., 2021]; larger microcolonies maintain acidic pH (below 5.5) within the biofilm than smaller ones [Xiao et al., 2017]. EPS-enmeshed microcolonies create localized acidic microenvironments at the biofilm/tooth enamel interface and consequently initiate demineralization of the tooth enamel or “white spots” carious lesions [Koo et al., 2013]. Eventually, the cross-kingdom biofilm leads to the aggressive onset of dental caries in an ECC rodent model under a sucrose-rich diet [Falsetta et al., 2014]. Thus, finding strategies to help control this virulent biofilm is essential.

Farnesol, a naturally occurring sesquiterpene alcohol, disrupts *S. mutans* cell membranes by increasing proton permeability, impairing acidogenicity, acid tolerance, and extra-/intra-cellular polysaccharides (EPS/IPS) synthesis without specific gene inhibition [Inoue et al., 2004; Koo et al., 2005; Rowat et al., 2005; Jeon et al., 2011]. In particular, the EPS protect the embedded microbes, thereby making them recalcitrant to antimicrobials [Bowen & Koo, 2011; Koo et al., 2013]. Meanwhile, farnesol is a *C. albicans* quorum-sensing

(QS) molecule that can prevent yeast-to-hypha transformation [Langford et al., 2009; Egbe et al., 2017]. Furthermore, the hyphal forms of *C. albicans* are distinctive in matured cross-kingdom biofilms, implying that hyphal development is relevant to an increase in biomass and the overall biofilm architecture [Falsetta et al., 2014; Hwang et al., 2017]. The hyphal transition of *C. albicans* assists vertical development of the dual-species biofilm [Kim et al., 2021], building a "drug trapping matrix" that prevents uptake and subcellular localization of antifungal agents in cooperation with *S. mutans*-derived EPS, formed on the surrogate *C. albicans* surface [Kim et al., 2018]. Thus, farnesol can be used for a dual-action on microorganisms to inhibit the bacterial cell membrane functions while simultaneously suppressing the fungal hyphal shift. However, farnesol cannot achieve maximal efficacy for biofilm treatment due to its hydrophobicity and poor biofilm retention if not combined with other modalities [Rocha et al., 2018].

Recent approaches to enhance anti-biofilm efficacies include a synergistic combination of fungal killing and matrix inhibition, catalytic nanoparticles, and drug delivery nanocarriers. A combination therapy (EPS inhibitor povidone-iodine with antifungal fluconazole) for the cross-kingdom biofilm treatment suppressed *C. albicans* carriage and mixed-biofilm formation without increasing bacterial killing activity *in vivo* [Kim et al., 2018]. Another approach employs a bi-functional nanohybrid system (Dex-IONP-Gox) that exploits the pathological conditions (i.e., high sucrose environment, low pH, and high EPS amounts) and triggers reactive oxygen species generation, killing *S. mutans* within a dual-species biofilm (*S. mutans* and commensal bacteria) [Huang et al., 2021]. Moreover, recent works have achieved efficient farnesol delivery against *S. mutans* biofilms using polymeric nanoparticle carriers (NPCs) [Horev et al., 2015; Zhou et al., 2016].

Polymeric nanoparticles have advantages, such as high stability in the body or for storage and increased biocompatibility [Dos Santos Ramos et al., 2018; Simon-Soro et al., 2021]. These polymeric NPCs loaded with farnesol have high adsorption affinities to pellicle and EPS-coated hydroxyapatite (HA) discs. Tertiary cationic surface residues enable farnesol-loaded NPCs to bind to pellicle and/or biofilms until the pH becomes acidic (below 5.5), and subsequently, the drug is released through protonation-mediated destabilization [Horev et al., 2015]. This pH-triggered "smart release" contributes to selective anti-biofilm efficacy, which may reduce off-target, chronic effects by targeting the specific pathogenic microenvironments, exactly when and where needed most [Liu, Ren, et al., 2018; Benoit et al., 2019]. We further advanced farnesol delivery *via* polymeric NPCs as saturated farnesol-NPC formulations, which improved drug loading capacity, extended drug release, and enhanced *S. mutans* biofilm disruption compared to standard drug formulations [Sims et al., 2019]; however, these results were all obtained using single-species *S. mutans* biofilm models. Efficacy elucidation using multi-species biofilm models mimicking ECC conditions (i.e., dual-species biofilm models of *S. mutans* and *C. albicans*) is more clinically relevant and critical for advancing and clinical translation of novel anti-biofilm strategies.

Here, we hypothesize that polymeric NPCs loaded with saturated farnesol (NPC+Far) can exert anti-biofilm activity by dual targeting both *S. mutans* and *C. albicans*. NPC+Far treatment reduced microbial cell viability and completely inhibited acid production of the biofilm. High-resolution confocal images further confirmed disrupted microcolony

formation of *S. mutans* and no hyphal development of *C. albicans*, hampering the biofilm 3D structure on NPC+Far-treated human teeth enamel (HT) slabs. Using transverse microradiography (TMR), we demonstrated that HT surfaces underneath the biofilms were almost intact in the NPC+Far treatment group. Our data revealed that NPC+Far application suppressed cariogenic bacterial-fungal accumulation, protecting enamel surfaces from demineralization, which may lead to a practical biofilm-targeting therapy for the prevention of ECC.

Methods

Preparation of farnesol-loaded polymeric nanoparticle carriers

Unless otherwise noted, all materials were supplied by Sigma-Aldrich. The pH-responsive polymer NPCs were formed from diblock copolymers using previously published methods [Horev et al., 2015; Zhou et al., 2016; Sims et al., 2019]. Briefly, a cationic corona block composed of poly(dimethylaminoethyl methacrylate), or p(DMAEMA), was synthesized *via* reversible addition-fragmentation chain transfer (RAFT) polymerization. For the hydrophobic core block, poly(dimethylaminoethyl methacrylate)-*b*-poly(dimethylaminoethyl methacrylate-*co*-butyl methacrylate-*co*-propylacrylic acid), or p(DMAEMA)-*b*-p(DMAEMA-*co*-BMA-*co*-PAA), was synthesized using RAFT polymerization. After forming diblock copolymers, NPCs were loaded with *tt*-farnesol (referred to as farnesol hereafter) as described previously [Sims et al., 2019]. Briefly, farnesol/PBS emulsions at 1.0 mg/mL were prepared using tip sonication (Fisher Scientific Sonic Dismembrator Model 100 at 4 W power setting) for ~30 seconds and immediately added to pre-weighed lyophilized diblock copolymers to achieve desired polymer NPC concentrations (0.5 mg/mL) in 20 mL glass scintillation vials. These solutions were sonicated (VWR 50 T Ultrasonic Cleaner) for 15 minutes to enable drug loading. NPC loading with farnesol was confirmed and measured *via* high performance liquid chromatography (HPLC). The quantification of loaded farnesol was used to calculate drug loading efficiency ($100\% \times (Wt_{loaded})/ Wt_0$) and drug loading capacity ($100\% \times (Wt_{loaded}/ Wt_{NPC} + Wt_{loaded})$) where Wt_{loaded} is the amount of loaded drug, Wt_0 is the initial amount of drug used, and Wt_{NPC} is the amount of polymer used.

Molecular weight and composition determination

Number average molecular weight (M_n) and polydispersity (PDI) of Block 1 and diblock copolymers was determined by gel permeation chromatography (GPC, Shimadzu Technologies) using a multi-angle light scattering detector (miniDAWN TREOS, Wyatt Technology) and a refractive index detector (Optilab T-rEX, Wyatt Technology). High Performance Liquid Chromatography (HPLC) grade DMF containing 0.05 M LiCl (0.2 μm PTFE filtered, Pall Corporation) and used as the mobile phase at a flow rate of 0.35 mL min^{-1} through a TSKgel SuperH-H guard column and either a TSKgel SuperHM-N or a TSKgel SuperAW2500 analytical column (Tosoh Biosciences) kept at 60 °C. ASTRA® 6.1 light scattering software (Wyatt Technology) and a previously reported dn/dc value (i.e., 0.06 for Block 1 and Block 2) [Vesterinen et al., 2011; Gallow et al., 2012] were used to determine molecular weight. CCR was determined from these values by calculating the Block 2 M_n (i.e., subtracting the Block 1 and Nexus Block M_n values from the recorded

triblock M_n) and dividing the Block 1 M_n by the result. Diblock copolymer composition was characterized by proton nuclear magnetic resonance (^{1}H NMR) using $CDCl_3$ as the solvent. As described below, the Block 1 DMAEMA plus the Block 2 DMAEMA, BMA, and PAA peaks were analyzed using established methods in accordance with known spectra [Convertine et al., 2009; Convertine et al., 2010; Li et al., 2013; Zheng et al., 2015; Fernando et al., 2018] to determine the polymer composition within Block 2:

^{1}H NMR of p(DMAEMA) and Block 2 DMAEMA: δ (ppm, from $CHCl_3$ signal at 7.26 ppm) 0.8–1.1 (3H, br m, CH_3–C), 1.8–1.9 (2H, br s, CH_2-C), 2.33 (3H, br s, N-CH_3), 2.6 (2H, br s, N-CH_2), 4.07 (2H, br s, CH_2-O-C=O).

^{1}H NMR of Block 2 BMA: δ (ppm, from $CHCl_3$ signal at 7.26 ppm) 0.9–1.02 (3H, br s, CH_3-C), 1.03 (2H, br s, C**H$_2$**-CH_3), 1.5 (2H, br s, CH_2-C**H$_2$**-CH_2), 1.8–1.9 (2H, br s, CH_2-C), 3.93 (2H, br s, CH_2-O-C=O).

^{1}H NMR of Block 2 PAA: δ (ppm, from $CHCl_3$ signal at 7.26 ppm) 0.85 (3H, br s, C**H$_3$**-CH_2), 1.4 (2H, br s, CH_2-C**H$_2$**-C), 1.5 (2H, br s, CH_2-C), 1.6 (2H, br s, C**H$_2$**-CH_3).

NPC self-assembly and characterization of size, polydispersity, and zeta potential

Diblock copolymers (Fig. 1) were self-assembled by adding either DDH_2O or PBS and bath sonicating (VWR 50 T Ultrasonic Cleaner) to the solution for 15 minutes. Size, polydispersity index (PDI), and zeta (ζ) potential were determined via dynamic light scattering (DLS) or zeta potential analysis using a Malvern Zetasizer NanoZS (Malvern Panalytical). Polymer concentrations of ~0.2–0.5 mg mL^{-1} in 90:10 DDH_2O:PBS solutions were filtered (0.45 μm PVDF, Perkin Elmer) into disposable cuvettes or p1070 capillary cells (Malvern Panalytical) and underwent General Purpose analysis in the Malvern Zetasizer software as previously described [Sims et al., 2019].

Microorganisms and growth conditions

Streptococcus mutans UA159 serotype c (an established cariogenic dental pathogen) and *Candida albicans* SC5314 (a well-characterized fungal strain) were used to generate co-species biofilms. For inoculum preparation, *C. albicans* (containing predominantly yeast cell forms) and *S. mutans* cells were grown to mid-exponential phase in ultrafiltered (10 kDa molecular-mass cutoff membrane; Millipore, MA, USA) tryptone-yeast extract broth (UFTYE; 2.5% tryptone and 1.5% yeast extract; pH 5.5 and 7.0 for *C. albicans* and *S. mutans*, respectively) with 1% (wt/vol) glucose at 37 °C and 5% CO_2 as described previously [Falsetta et al., 2014; Hwang et al. 2017].

In vitro biofilm model on sHA and sHT

Biofilms were formed on saliva-coated hydroxyapatite (sHA) discs or human tooth enamel (sHT) slabs, as described previously [Xiao et al., 2017; Kim et al., 2018; Liu, Naha, et al., 2018]. Briefly, sHA discs (surface area = 2.7 ± 0.2 cm^2; Clarkson Chromatography Products, Inc., South Williamsport, PA) were vertically suspended in 24-well plates using a custom-made wire disc holder while sHT slabs (4mm × 4 mm) were mounted vertically in 48-well plates, mimicking the smooth surfaces of the pellicle-coated teeth. Each sHA disc

or sHT slab was inoculated with approximately 2×10^6 (colony-forming units (CFU)/mL) of *S. mutans* and 2×10^4 (CFU/mL) of *C. albicans* in UFTYE (pH 7.0) containing 1% (wt/vol) sucrose at 37 °C under 5% CO_2; the microorganisms share similar proportion with that found in saliva samples from children with ECC [Falsetta et al., 2014; Xiao et al., 2016]. The culture medium was changed twice daily at 8 am and 6 pm until the end of the experimental period.

Biofilm treatment and quantitative analysis

The biofilms were topically treated with four treatment solutions: free nanoparticles (NPC; 0.5 mg/mL in PBS, pH 7.0), farnesol-loaded nanoparticles (referred to as NPC+Far hereafter, 0.5 mg/mL loaded with 1.0 mg/mL farnesol, in PBS, pH 7.0), free farnesol (Far; 1.0 mg/mL farnesol, in PBS, pH 7.0), vehicle control PBS (pH 7.0). For each treatment, the biofilms were subjected to the above-described solutions for 2.5 min with 2.5-min intervals (total of 10 min-exposure/treatment) and then transferred to a fresh culture medium. Specifically, 25 μL or 12.5 μL NPC and drug solutions were applied to each side of each disc or slab, respectively, at 0, 2.5, 5, and 7.5 minutes with a total application volume of 400 μL for each pair of discs and 200 μL for each pair of slabs. The first treatment was applied directly after salivary pellicle formation (sHA/sHT), and the treated discs or enamel slabs were transferred to the inoculated culture medium. Biofilms were allowed to form on the discs or enamel slabs without interruption for 6 hours, at which point a second treatment was applied. After the second treatment, the biofilms were returned to the same culture medium. The next day, biofilms on sHA were treated three times (8 am, 2 pm, and 8 pm) at 20, 26, and 32 h of the experimental period, and the culture media was changed twice (at 20 h and 30 h) (Fig. 2a). After 44 h, the biofilms were collected and analyzed as described below. For sHT slabs, the biofilms were treated twice daily (8 am and 6 pm) to (1) highlight the differences in enamel sub-surface demineralization among groups and (2) simulate a clinically-relevant regimen, and the cultivation period was prolonged by 67 h so that sub-surface demineralization of enamel can be clearly observed and evaluated (Fig. S1a). For quantitative analyses, the biofilms were removed from sHA or sHT and homogenized by sonication (water bath sonication followed by probe sonication for 30 s pulse at an output of 7 W; Branson Sonifier 150, Branson Ultrasonics, Danbury, CT, USA), providing optimum dispersal and maximum recoverable counts in our biofilm model without killing bacterial cells [Koo et al., 2003; Koo et al., 2005; Xiao et al., 2012]. The homogenized suspension was partially used to determine the total number of viable cells in each of the treated biofilms by colony forming units (CFU). The remaining biofilm suspension was washed twice with Milli-Q water, oven-dried for 2 h, and weighed to obtain biomass (insoluble dry-weight).

Visualization of 3D biofilm architecture

To examine the impact of NPC+Far treatment on the 3D architecture of the biofilms on the sHT slabs, we used high-resolution confocal microscopy with optimized protocols for biofilm imaging and quantification [Kim et al., 2018; Liu, Naha, et al., 2018]. Briefly, EPS glucans were labeled *via* incorporation of 1 μM Alexa Fluor 647 dextran conjugate (absorbance/fluorescence emission maxima of 647/668 nm; Molecular Probes Inc., Eugene, OR, USA) during biofilm formation. *S. mutans* cells were stained with

2.5 μM SYTO 9 green-fluorescent nucleic acid stain (485/498 nm; Molecular Probes Inc.) while *C. albicans* cells were stained using concanavalin A (ConA) lectin conjugated with tetramethylrhodamine at 40 μg/ml (555/580 nm; Molecular Probes Inc.). The biofilm imaging was performed using an upright single-photon confocal microscope (LSM800, Zeiss, Jena, Germany) equipped with a 20 × (numerical aperture = 1.0) water immersion objective. Each component was illuminated sequentially to minimize cross-talk as follows: SYTO 9 was excited using 488 nm and collected by a 480/40 nm emission filter; ConA was excited using 560 nm and collected by a 560/40 nm emission filter; Alexa Fluor 647 was excited using 640 nm and collected by a 670/40 nm emission filter. Images were acquired from at least three randomly selected spots of each sample. Image J software (version 1.48) was used to create 3D renderings of biofilm architecture.

Glycolytic pH-drop assay

The effects of NPC+Far treatment on acidogenicity/aciduricity of the cross-kingdom biofilm were measured by the glycolytic pH-drop assay, as described previously [Jeon et al., 2011]. Briefly, 20 h biofilms on sHA with 3-time treatments (at 0 h, 6 h, and 20 h) (Fig. 2a) were washed with salt solution (50 mM KCl plus 1 mM $MgCl_2$, pH 7.0) and were starved for 1 h by immersing in 20 mM potassium phosphate buffer, followed by resuspension in a fresh salt solution (adjusted to pH 7.2). Glucose was added to the solution at a final concentration of 1% (wt/vol), and the decrease in pH was measured using a pH electrode for 120 min at 10 min intervals (Thermo Scientific, Waltham, MA, USA). Biofilms on sHT for the glycolytic pH-drop assay were incubated for 67 hours, during which time they were treated twice daily (Fig. S1a) because the pH of spent media for sHT showed a different trend than that of sHA (Fig. S2), requiring more frequent treatments. The subsequent process was the same as for sHA as described above.

Demineralization Analysis: TMR

After 3D biofilm structure acquisition, the biofilms on the HT slabs were removed by sonication and further treated with enzymes to avoid scratching their surfaces. Briefly, HT slabs were transferred to the mixture of dextranase and mutanase (pH 5.5; 6.25 U and 1.25 U, respectively) for a 2 h incubation with rocking at 37 °C, followed by washing with Milli-Q water. The collected specimens were mounted on plastic rods and sectioned with a hard tissue microtome (Silverstone-Taylor Hard Tissue Microtome, Series 1000 Deluxe) for transversal microradiography (TMR). One 100 μm section was obtained from the center of each specimen, mounted on X-ray sensitive plates (Microchrome Technology), and subjected to X-ray, along with an aluminum step wedge. Inspektor TMR 2000 (ver. 1.25, Inspektor Research Systems BV, Amsterdam, The Netherlands) was used to analyze microradiographic images with sound enamel defined at 87% mineral volume to obtain mean lesion depth (μm) [Xiao et al., 2017; Liu, Naha, et al., 2018].

Statistical analysis

The results are expressed as means ± standard deviations (s.d.). For multiple comparisons, one-way analysis of variance (ANOVA) with Dunnett's multiple comparisons test or Kruskal-Wallis test with Dunn's multiple comparisons test was performed to detect any statistical differences among the group. For any pairwise comparison, Student's *t*-test with

Welch's correction was conducted. The significant levels were set at 5%. GraphPad Prism version 5.0d for Mac OS X (GraphPad Software, San Diego, CA) was used to perform statistical analyses.

Results

Recent work successfully demonstrated enhanced antibacterial effectiveness against planktonic and biofilm *S. mutans* using a novel saturated drug-loaded NPC formulation approach [Sims et al., 2019]. Based on previous findings that showed NPCs with corona-to-core molecular weight ratios of ~3.5–4 and small diameters (≤ ~20 nm) exhibited higher antibacterial effectiveness [Zhou et al., 2016; Sims et al., 2019], we used NPCs bearing these characteristics for this investigation. As depicted in Fig. 1, diblock copolymers that were synthesized using reversible addition fragmentation chain transfer (RAFT) polymerization and were capable of self-assembling into NPCs were used to load and deliver farnesol to the biofilms. In particular, the NPCs used had an overall molecular weight (M_n) of 16.2 kDa, a corona-to-core molecular weight ratio of 3.6, a diameter of 18.6 nm, and a zeta potential of 19.7 mV (Table 1). The core block for these NPCs contained 37% DMAEMA, 57% BMA, and 6% PAA (Table 1). These NPCs demonstrated drug loading efficiency of 85.8% and drug loading capacity of 63.2% when loaded with saturated farnesol (Fig. 1).

NPC+Far is a potential inhibitor of single *S. mutans* biofilm [Horev et al., 2015; Zhou et al., 2016; Sims et al., 2019]. Thus, to investigate whether NPC+Far treatment is effective against *S. mutans-C. albicans* biofilm, we analyzed cell viability and total biomass using the sHA-biofilm model with a topical treatment regimen simulating clinical conditions (Fig. 2a). As a result, NPC+Far treatment potently reduced microbial cell viability (CFU/mL) in biofilms by approximately 2 logs of both *S. mutans* and *C. albicans*, whereas other treatments showed no reduction in CFUs (Fig. 2b). Furthermore, NPC+Far significantly reduced biomass (total dry weight) compared with PBS, NPC, or Far alone (Fig. 2c).

Next, the influence of NPC+Far on acidification-related activities of *S. mutans-C. albicans* biofilm was determined by a glycolytic pH-drop assay in which the rate of pH drop reflects acidogenicity, while final pH values represent aciduricity [Gregoire et al., 2007]. Although an immediate pH-drop was detected in PBS, NPC, or Far after 1% glucose supplement, the pH values in NPC+Far sustained at around pH 7, suggesting NPC+Far strongly inhibited acidification-related activities in our biofilm model (Fig. 2d). Our preliminary experiments showed that the pH of spent culture media did not indicate biofilm acidification, especially in the sHA model, because cells detached from the biofilm can grow within the wells, lowering the culture pH (Fig. S2).

To evaluate the anti-biofilm effects of NPC+Far under oral-mimetic conditions, we further analyzed (1) each dual-species biofilm architecture formed on saliva-coated human tooth enamel (sHT) slabs and (2) post-treated enamel demineralization beneath the biofilms. High-resolution confocal imaging demonstrated that NPC+Far treatment substantially reduced EPS matrix, impaired *S. mutans* microcolony formation, and inhibited *C. albicans* hyphal transformation (Fig. 3a), congruent with preliminary microbiological and biochemical data using HT slabs, such as significant reduction of cell numbers and biomass, and

attenuated acidogenicity (Fig. S1). Moreover, neither “white spot” lesions nor subsurface demineralization were observed when the biofilms on HT were treated with NPC+Far, whereas PBS, NPC, or Far treatment showed obvious “white-spot-like” patterns and subsurface caries-like lesions (Fig. 3b, 3c). Table 2 includes the quantitative assessment of HT demineralization, analyzed by transverse microradiography (TMR). NPC+Far treatment provided the greatest effect, with a 79% reduction in lesion depth (5.5 ± 3.4 μm) and an 85% decrease in mineral loss (98 ± 77 vol%.μm) *versus* those in PBS (26.2 ± 18.9 μm in lesion depth and 640 ± 412 vol%.μm in mineral loss, respectively). On the other hand, no significant differences were detected among PBS, NPC, and Far. These results suggest that improved farnesol delivery by NPCs inhibits bacterial-fungal accumulation and acidification, resulting in enamel surface protection.

Discussion

The chemotherapeutic control of cross-kingdom biofilms is challenging because they display enhanced tolerance to antimicrobials resulting from their structural complexity [Kong et al., 2016; Townsend et al., 2017]. To address the recalcitrant cross-kingdom biofilm, we employed NPC-based drug delivery combined with a saturated farnesol formulation (NPC+Far; Fig. 1a). Here, we show NPC+Far can potentiate anti-biofilm activity by dual targeting towards (1) *S. mutans* cell membrane functions involving cariogenic virulence and (2) *C. albicans* hyphal formation relevant to the overall biofilm architecture, and thereby can protect human tooth enamel from acidic dissolution.

NPCs with farnesol encapsulated within disrupts *S. mutans* biofilm formation [Horev et al., 2015; Zhou et al., 2016], which is further boosted by combining with a saturated drug formulation [Sims et al., 2019]. Furthermore, NPCs combined with a saturated drug formulation are more potent than NPCs with a standard drug formulation, showing high farnesol loading capacity (~300%), extended drug release duration (3-fold), and amplified antibacterial effects against *S. mutans*-single biofilms [Sims et al., 2019]. NPC+Far was synthesized to be the same NPCs employed in Sims’s study and had nearly identical characteristics for most categories (Table 1); hence, they can be valid to consider as the equivalent. In line with the previous study, a saturated formulation (NPC+Far), employed here, exerted considerable anti-biofilm activity against the cross-kingdom biofilms; the substantial reductions in dry weight and cell viability (–2 logs) in the NPC+Far group (Figs. 2b, c and S1b, c). Given that our biofilm model mimicks the worst cariogenic scenario, even a 2-log decrease in CFUs could affect the pathogenicity of the biofilm. The remaining cells would disperse to restart the biofilm lifecycle (Kaplan 2010). The single dispersed cells are susceptible to antibiotics (Koo et al., 2017), suggesting that specific and clinically applied regimens can hamper biofilm rebuilding. Moreover, NPC+Far showed 52-fold and 40-fold greater cell reduction in *S. mutans* and *C. albicans*, respectively, and exhibited 18-fold higher biomass reduction than a standard formulation (NPC+StdFar) (Table S1). These findings could explain that NPC+Far thwarted biofilm accumulation and successfully prevented enamel surface damage (Fig. 3), whereas free farnesol (Far) proved ineffective as PBS or free NPC. Our observation indicates that, in this “hypervirulent” model, which is not the case in several published works [Langford et al., 2010; Fernandes et al., 2016; Polke et al., 2018], the effect of free farnesol could be surpassed by the synergistic interaction of

the bacterium and the fungus mediated mainly by bacterial EPS that can cover the cells and impede the access of farnesol to cells, resulting in the ineffectiveness of free farnesol against the biofilm model.

Furthermore, NPC+Far treatment could impair biofilm maturation by inhibiting *C. albicans*-derived structural framework that supports the EPS shield. Our data reveal that treatment with NPC+Far dramatically altered biofilm formation and 3D architecture on sHT; NPC+Far-treated biofilm exhibited sparse yeast cells of *C. albicans* (no hyphal form), significantly less EPS, and smaller *S. mutans* microcolonies (Fig. 3a). Our preliminary analysis using sHA disc model revealed that Far-treated biofilm clearly exhibited only yeast form of *C. albicans* and showed as large microcolonies of *S. mutans* and copious EPS as PBS- or NPC-treated group (Fig. S3), indicating these preventive outcomes could be caused both by the impaired hyphal formation of *C. albicans* and cell membrane functions in *S. mutans* rather than antimicrobial adhesions. However, the impact of NPC+Far on microbial adhesion needs further elucidation. Interestingly, we also observed sustained higher pH values (> pH 6.4) in spent culture media of sHA than those of sHT (Fig. S2). Further studies should be conducted to provide definitive evidence for the discrepancies; nevertheless, it is clear that the sHT model allows us to scrutinize the efficacy of NPC-based drug delivery on ECC biofilm, giving us a better understanding of potential clinical outcomes. These findings agree with the well-defined mechanisms of farnesol targeting bacterial-fungal components [Langford et al., 2009; Jeon et al., 2011], which potentially provide more drug penetration to the biofilm/tooth enamel interface, preventing the dual-species biofilm from maintaining localized acidic pH at the enamel surface.

The enamel surfaces attached by *S. mutans*-*C. albicans* biofilms were demineralized more severely than those by *S. mutans*-single biofilms [Kim et al., 2021], partly reflecting frequent *C. albicans* detection in plaque from ECC children afflicted with rampant caries. Indeed, children with oral *C. albicans* have higher odds (> 5 times) of experiencing ECC than those without *C. albicans* [Xiao et al., 2018]. Here, we also investigated the efficacy of NPC+Far using sHT model that mimics ECC-like biofilm formed on human tooth enamel. The sHT surface from NPC+Far treatment remained almost intact, whereas those from other treatment agents exhibited “white-spot-like” patterns (Fig. 3b). Also, corresponding with these visual differences, the greatest effect of NPC+Far on the reduction of enamel demineralization (lesion depth and mineral loss; Table 2) was quantitatively confirmed among the tested agents.

Caries-preventive outcomes were related to the glycolytic activities (acidogenicity/aciduricity) of biofilms [Jeon et al. 2011]. As indicated by the rate of pH drop (Fig. 2d, Fig. S1d), effectively delivered farnesol *via* NPCs disrupted both the acidogenic and aciduric activities of the microbial cells in the biofilm, most likely *S. mutans* cells. We further observed NPC+Far slightly disrupted glycolytic activities on pre-formed (20 h) biofilms (Fig. S4), suggesting NPC+Far can exert direct inhibition to pre-formed biofilms to some extent, consistent with previous studies [Koo et al., 2003; Jeon et al., 2011], as well as prevent cell accumulation by cumulative treatment effects.

Evaluation of the drug efficacy under oral- and clinical-mimetic conditions, including brief drug exposures, is imperative to the successful clinical adoption of biofilm treatment agents. Unlike our drug application, continuous free-farnesol treatment indeed inhibits *S. mutans-C. albicans* biofilm formation [Fernandes et al., 2016]; however, this anti-biofilm activity has been achieved by 48 h exposure to free farnesol, not intermittent, as it occurs in clinical situations. On the other hand, in our study, the biofilms were treated only for 10 min under a twice- or three times-daily topical treatment regimen, simulating clinically-relevant oral use (Figs. 2a and S1a). However, some limitations are worth noting.

The efficacy of the nanotechnology-based drug delivery *in vitro* needs further validation. Although the 3D organization clearly shows that the strategy was adequate to impede biofilm accumulation, accurate total biomass requires biovolume or insoluble exopolysaccharides quantification. Our study has not solved the technical problems inherent in thick, matured biofilms (e.g., lack of adequate laser penetration for good fluorescence signal to gather information without distortion); therefore, experimental design needs to be optimized for the subsequent study. It is also noteworthy that farnesol-treated *C. albicans* biofilms showed susceptibility to antifungals as well as hyphal growth inhibition through cAMP pathway genes [Chen et al., 2018], indicating the antibiofilm performance of NPC+Far can be further enhanced by combining it with conventional antifungals without increasing bacterial killing activity and hence, reducing influence on the oral microbial community.

Altogether, the present study provides new insights to combat cariogenic *S. mutans-C. albicans* biofilm using nanotechnology-based drug delivery. In our model, NPC+Far treatment inhibited 3D biofilm organization and disrupted acidification-related activities, thereby preventing localized demineralization (caries-like lesions) on human tooth-enamel from the highly virulent bacterial-fungal biofilm. This work may enhance a clinically relevant and meaningful regimen for controlling pathogenic biofilms associated with the prevalent and costly ECC and thereby could help promote oral health in children.

Supplementary Material

Refer to Web version on PubMed Central for supplementary material.

Acknowledgments

The authors gratefully acknowledge the National Institutes of Health (R01 DE018023 and R01 DE02584) and the São Paulo Research Foundation (Fundação de Amparo à Pesquisa do Estado de São Paulo - FAPESP #2018/26441-7). Though research reported in this publication was supported by the National Institute of Dental & Craniofacial Research of the National Institutes of Health, the content is solely the responsibility of the authors and does not necessarily represent the official views of the National Institutes of Health.

Statement of ethics

The whole saliva was collected to coat the hydroxyapatite discs or human tooth enamel slabs for the *in vitro* biofilm studies. The experimental protocol was reviewed and approved by the University of Pennsylvania Research Subject committee (IRB#818549). All subjects' rights were protected, and informed consent was granted in writing.

References

Benoit DS, & Koo H (2016). Targeted, triggered drug delivery to tumor and biofilm microenvironments. Nanomedicine, 11, 873–879. doi: 10.2217/nnm-2016-0014. [PubMed: 26987892]

Benoit DSW, Sims KR Jr., & Fraser D (2019). Nanoparticles for Oral Biofilm Treatments. ACS Nano, 13, 4869–4875. doi: 10.1021/acsnano.9b02816. [PubMed: 31033283]

Bowen WH, & Koo H (2011). Biology of *Streptococcus mutans*-derived glucosyltransferases: role in extracellular matrix formation of cariogenic biofilms. Caries Research, 45, 69–86. doi: 10.1159/000324598.

Chen S, Xia J, Li C, Zuo L, & Wei X (2018). The possible molecular mechanisms of farnesol on the antifungal resistance of *C. albicans* biofilms: the regulation of CYR1 and PDE2. BMC Microbiology, 18, 203. doi: 10.1186/s12866-018-1344-z. [PubMed: 30509171]

Convertine AJ, Benoit DS, Duvall CL, Hoffman AS, & Stayton PS (2009). Development of a novel endosomolytic diblock copolymer for siRNA delivery. J Control Release, 133, 221–229. doi: 10.1016/j.jconrel.2008.10.004. [PubMed: 18973780]

Convertine AJ, Diab C, Prieve M, Paschal A, Hoffman AS, Johnson PH, & Stayton PS (2010). pH-responsive polymeric micelle carriers for siRNA drugs. Biomacromolecules, 11, 2904–2911. doi: 10.1021/bm100652w. [PubMed: 20886830]

de Carvalho FG, Silva DS, Hebling J, Spolidorio LC, & Spolidorio DM (2006). Presence of mutans streptococci and *Candida* spp. in dental plaque/dentine of carious teeth and early childhood caries. Archives of Oral Biology, 51, 1024–1028. doi: 10.1016/j.archoralbio.2006.06.001. [PubMed: 16890907]

Dos Santos Ramos MA, Da Silva PB, Spósito L, De Toledo LG, Bonifácio BV, Rodero CF, Dos Santos KC, Chorilli M, & Bauab TM (2018). Nanotechnology-based drug delivery systems for control of microbial biofilms: a review. International Journal of Nanomedicine, 13, 1179–1213. doi: 10.2147/IJN.S146195. [PubMed: 29520143]

Egbe NE, Dornelles TO, Paget CM, Castelli LM, & Ashe MP (2017). Farnesol inhibits translation to limit growth and filamentation in *C. albicans* and *S. cerevisiae*. Microbial Cell, 4, 294–304. doi: 10.15698/mic2017.09.589. [PubMed: 28913344]

Falsetta ML, Klein MI, Colonne PM, Scott-Anne K, Gregoire S, Pai CH, Gonzalez-Begne M, Watson G, Krysan DJ, Bowen WH, & Koo H (2014). Symbiotic relationship between *Streptococcus mutans* and *Candida albicans* synergizes virulence of plaque biofilms *in vivo*. Infection and Immunity, 82, 1968–1981. doi: 10.1128/IAI.00087-14. [PubMed: 24566629]

Fernandes RA, Monteiro DR, Arias LS, Fernandes GL, Delbem AC, & Barbosa DB (2016). Biofilm formation by *Candida albicans* and *Streptococcus mutans* in the presence of farnesol: a quantitative evaluation. Biofouling, 32, 329–338. doi: 10.1080/08927014.2016.1144053. [PubMed: 26905659]

Fernando LP, Lewis JS, Evans BC, Duvall CL, & Keselowsky BG (2018). Formulation and characterization of poly(propylacrylic acid)/poly(lactic-co-glycolic acid) blend microparticles for pH-dependent membrane disruption and cytosolic delivery. Journal of Biomedical Materials Research Part A, 106, 1022–1033. doi: 10.1002/jbm.a.36298. [PubMed: 29164777]

Gallow KC, Jhon YK, Genzer J, & Loo YL (2012). Influence of gradient strength and composition profile on the onset of the cloud point transition in hydroxyethyl methacrylate/dimethylaminoethyl methacrylate gradient copolymers. Polymer, 53, 1131–1137. doi: 10.1016/j.polymer.2012.01.027.

Gregoire S, Singh AP, Vorsa N, & Koo H (2007). Influence of cranberry phenolics on glucan synthesis by glucosyltransferases and *Streptococcus mutans* acidogenicity. Journal of Applied Microbiology, 103, 1960–1968. doi: 10.1111/j.1365-2672.2007.03441.x. [PubMed: 17953606]

Hajishengallis E, Parsaei Y, Klein MI, & Koo H (2017). Advances in the microbial etiology and pathogenesis of early childhood caries. Molecular Oral Microbiology, 32, 24–34. doi: 10.1111/omi.12152. [PubMed: 26714612]

Horev B, Klein MI, Hwang G, Li Y, Kim D, Koo H, & Benoit DS (2015) pH-activated nanoparticles for controlled topical delivery of farnesol to disrupt oral biofilm virulence. ACS Nano, 9, 2390–2404. doi: 10.1021/nn507170s. [PubMed: 25661192]

Huang Y, Liu Y, Shah S, Kim D, Simon-Soro A, Ito T, Hajfathalian M, Li Y, Hsu JC, Nieves LM, Alawi F, Naha PC, Cormode DP, & Koo H (2021). Precision targeting of bacterial pathogen via bi-functional nanozyme activated by biofilm microenvironment. Biomaterials, 268, 120581. doi: 10.1016/j.biomaterials.2020.120581. [PubMed: 33302119]

Hwang G, Liu Y, Kim D, Li Y, Krysan DJ, & Koo H (2017). *Candida albicans* mannans mediate *Streptococcus mutans* exoenzyme GtfB binding to modulate cross-kingdom biofilm development *in vivo*. PLoS Pathogens, 13, e1006407. doi: 10.1371/journal.ppat.1006407. [PubMed: 28617874]

Inoue Y, Shiraishi A, Hada T, Hirose K, Hamashima H, & Shimada J (2004). The antibacterial effects of terpene alcohols on *Staphylococcus aureus* and their mode of action. FEMS Microbiology Letters, 237, 325–331. doi: 10.1016/j.femsle.2004.06.049. [PubMed: 15321680]

Jeon JG, Pandit S, Xiao J, Gregoire S, Falsetta ML, Klein MI, & Koo H (2011). Influences of trans-trans farnesol, a membrane-targeting sesquiterpenoid, on *Streptococcus mutans* physiology and survival within mixed-species oral biofilms. International Journal of Oral Science, 3, 98–106. doi: 10.4248/IJOS11038. [PubMed: 21485314]

Kaplan JB (2010). Biofilm Dispersal: Mechanisms, clinical implications, and potential therapeutic uses. Journal of Dental Research, 89, 205–218. doi: 10.1177/0022034509359403. [PubMed: 20139339]

Kim D, & Koo H (2020). Spatial Design of Polymicrobial Oral Biofilm in Its Native Disease State. Journal of Dental Research, 99, 597–603. doi: 10.1177/0022034520909313. [PubMed: 32142402]

Kim D, Liu Y, Benhamou RI, Sanchez H, Simón-Soro Á, Li Y, Hwang G, Fridman M, Andes DR, & Koo H (2018). Bacterial-derived exopolysaccharides enhance antifungal drug tolerance in a cross-kingdom oral biofilm. ISME Journal. 12, 1427–1442. doi: 10.1038/s41396-018-0113-1. [PubMed: 29670217]

Kim HE, Liu Y, Dhall A, Bawazir M, Koo H, & Hwang G (2021). Synergism of *Streptococcus mutans* and *Candida albicans* Reinforces Biofilm Maturation and Acidogenicity in Saliva: An *In Vitro* Study. Frontiers in Cellular and Infection Microbiology, 10, 623980. doi: 10.3389/fcimb.2020.623980. [PubMed: 33680985]

Kong EF, Tsui C, Kucharíková S, Andes D, Van Dijck P, & Jabra-Rizk MA (2016). Commensal Protection of *Staphylococcus aureus* against Antimicrobials by *Candida albicans* Biofilm Matrix. mBio, 7, e01365–16. doi: 10.1128/mBio.01365-16. [PubMed: 27729510]

Koo H, Andes DR, & Krysan DJ (2018). Candida-streptococcal interactions in biofilm-associated oral diseases. PLoS Pathogens, 14, e1007342. doi: 10.1371/journal.ppat.1007342. [PubMed: 30543717]

Koo H, Allan RN, Howlin RP, Stoodley P, & Hall-Stoodley L (2017). Targeting microbial biofilms: current and prospective therapeutic strategies. Nature Reviews Microbiology, 15, 740–755. doi: 10.1038/nrmicro.2017.99. [PubMed: 28944770]

Koo H, Falsetta ML, & Klein MI (2013). The exopolysaccharide matrix: a virulence determinant of cariogenic biofilm. Journal of Dental Research, 92, 1065–1073. doi: 10.1177/0022034513504218. [PubMed: 24045647]

Koo H, Hayacibara MF, Schobel BD, Cury JA, Rosalen PL, Park YK, Vacca-Smith AM, & Bowen WH (2003). Inhibition of *Streptococcus mutans* biofilm accumulation and polysaccharide production by apigenin and *tt*-farnesol. Journal of Antimicrobial Chemotherapy. 52, 782–789. doi: 10.1093/jac/dkg449. [PubMed: 14563892]

Koo H, Schobel B, Scott-Anne K, Watson G, Bowen WH, Cury JA, Rosalen PL, & Park YK (2005). Apigenin and *tt*-farnesol with fluoride effects on *S. mutans* biofilms and dental caries. Journal of Dental Research, 84, 1016–1020. doi: 10.1177/154405910508401109. [PubMed: 16246933]

Langford ML, Atkin AL, & Nickerson KW (2009). Cellular interactions of farnesol, a quorum-sensing molecule produced by *Candida albicans*. Future Microbiology, 4, 1353–1362. doi: 10.2217/fmb.09.98. [PubMed: 19995193]

Langford ML, Hasim S, Nickerson KW, & Atkin AL (2010). Activity and toxicity of farnesol towards *Candida albicans* are dependent on growth conditions. Antimicrobial Agents and Chemotherapy, 54, 940–942. doi: 10.1128/AAC.01214-09. [PubMed: 19933803]

Li Q, Bao Y, Wang H, Du F, Li Q, Jin B, & Bai R (2013). A facile and highly efficient strategy for esterification of poly(meth)acrylic acid with halogenated compounds at room

temperature promoted by 1,1,3,3-tetramethylguanidine. Polymer Chemistry, 4, 2891–2897. 10.1039/C3PY00155E.

Liu Y, Naha PC, Hwang G, Kim D, Huang Y, Simon-Soro A, Jung HI, Ren Z, Li Y, Gubara S, Alawi F, Zero D, Hara AT, Cormode DP, & Koo H (2018). Topical ferumoxytol nanoparticles disrupt biofilms and prevent tooth decay in vivo via intrinsic catalytic activity. Nature Communications, 9, 2920. doi: 10.1038/s41467-018-05342-x.

Liu Y, Ren Z, Hwang G, & Koo H (2018). Therapeutic Strategies Targeting Cariogenic Biofilm Microenvironment. Advances in Dental Research, 29, 86–92. doi: 10.1177/0022034517736497. [PubMed: 29355421]

Paes Leme AF, Koo H, Bellato CM, Bedi G, & Cury JA (2006). The role of sucrose in cariogenic dental biofilm formation--new insight. Journal of Dental Research, 85, 878–887. doi: 10.1177/154405910608501002. [PubMed: 16998125]

Polke M, Leonhardt I, Kurzai O, & Jacobsen ID (2018). Farnesol signalling in *Candida albicans* – more than just communication. Critical Reviews in Microbiology, 44, 230–243. doi: 10.1080/1040841X.2017.1337711. [PubMed: 28609183]

Raja M, Hannan A, & Ali K (2010). Association of oral candidal carriage with dental caries in children. Caries Research, 44, 272–276. doi: 10.1159/000314675. [PubMed: 20516688]

Rocha GR, Florez Salamanca EJ, de Barros A,L, Lobo CIV, & Klein MI (2018). Effect of *tt*-farnesol and myricetin on *in vitro* biofilm formed by *Streptococcus mutans* and *Candida albicans*. BMC Complementary and Alternative Medicine, 18, 61. doi: 10.1186/s12906-018-2132-x. [PubMed: 29444673]

Rowat AC, Keller D, & Ipsen JH (2005). Effects of farnesol on the physical properties of DMPC membranes. Biochimica et Biophysica Acta, 1713, 29–39. doi: 10.1016/j.bbamem.2005.04.014. [PubMed: 15963943]

Simon-Soro A, Kim D, Li Y, Liu Y, Ito T, Sims KR Jr, Benoit DSW, Bittinger K, & Koo H (2021). Impact of the repurposed drug thonzonium bromide on host oral-gut microbiomes. NPJ Biofilms Microbiomes, 7, 7. doi: 10.1038/s41522-020-00181-5. [PubMed: 33483519]

Sims KR, Liu Y, Hwang G, Jung HI, Koo H, & Benoit DSW (2018). Enhanced design and formulation of nanoparticles for anti-biofilm drug delivery. Nanoscale, 11, 219–236. doi: 10.1039/c8nr05784b. [PubMed: 30525159]

Townsend EM, Sherry L, Kean R, Hansom D, Mackay WG, Williams C, Butcher J, & Ramage G (2017). Implications of Antimicrobial Combinations in Complex Wound Biofilms Containing Fungi. Antimicrobial Agents and Chemotherapy, 61, e00672–17. doi: 10.1128/AAC.00672-17. [PubMed: 28696230]

Vesterinen A, Lipponen S, Rich J, & Seppälä J (2011). Effect of block composition on thermal properties and melt viscosity of poly(2-(dimethylamino)ethyl methacrylate), poly(ethylenen oxide) and poly(propylene oxide) block co-polymers. eXPRESS Polymer Letters, 5,754–765. doi: DOI: 10.3144/expresspolymlett.2011.74

Xiao J, Hara AT, Kim D, Zero DT, Koo H, & Hwang G (2017). Biofilm three-dimensional architecture influences in situ pH distribution pattern on the human enamel surface. International Journal of Oral Science, 9, 74–79. doi: 10.1038/ijos.2017.8. [PubMed: 28452377]

Xiao J, Huang X, Alkhers N, Alzamil H, Alzoubi S, Wu TT, Castillo DA, Campbell F, Davis J, Herzog K, Billings R, Kopycka-Kedzierawski DT, Hajishengallis E, & Koo H (2018). *Candida albicans* and Early Childhood Caries: A Systematic Review and Meta-Analysis. Caries Research, 52, 102–112. doi: 10.1159/000481833. [PubMed: 29262404]

Xiao J, Klein MI, Falsetta ML, Lu B, Delahunty CM, Yates JR 3rd, Heydorn A, & Koo H (2012). The exopolysaccharide matrix modulates the interaction between 3D architecture and virulence of a mixed-species oral biofilm. PLoS Pathogens, 8, e1002623. doi: 10.1371/journal.ppat.1002623. [PubMed: 22496649]

Xiao J, Moon Y, Li L, Rustchenko E,. Wakabayashi H, Zhao X, Feng C, Gill SR, McLaren S, Malmstrom H, Ren Y, Quivey R, Koo H, & Kopycka-Kedzierawski DT (2016). *Candida albicans* Carriage in Children with Severe Early Childhood Caries (S-ECC) and Maternal Relatedness. PLoS One, 11, e0164242. doi: 10.1371/journal.pone.0164242. [PubMed: 27741258]

Yang XQ, Zhang Q, Lu LY, Yang R, Liu Y, & Zou J (2012). Genotypic distribution of *Candida albicans* in dental biofilm of Chinese children associated with severe early childhood caries. Archives of Oral Biology, 57, 1048–1053. doi: 10.1016/j.archoralbio.2012.05.012. [PubMed: 22717324]

Zheng JY, Tan MJ, Thoniyot P, & Loh XJ (2015). Unusual thermogelling behaviour of poly[2-(dimethylamino)ethyl methacrylate] (PDMAEMA)-based polymers polymerized in bulk. RSC Advances, 5, 62314–62318. doi: 10.1039/C5RA12816A.

Zhou J, Horev B, Hwang G, Klein MI, Koo H, & Benoit DS (2016). Characterization and optimization of pH-responsive polymer nanoparticles for drug delivery to oral biofilms. Journal of Materials Chemistry B, 4, 3075–3085. doi: 10.1039/C5TB02054A. [PubMed: 27429754]

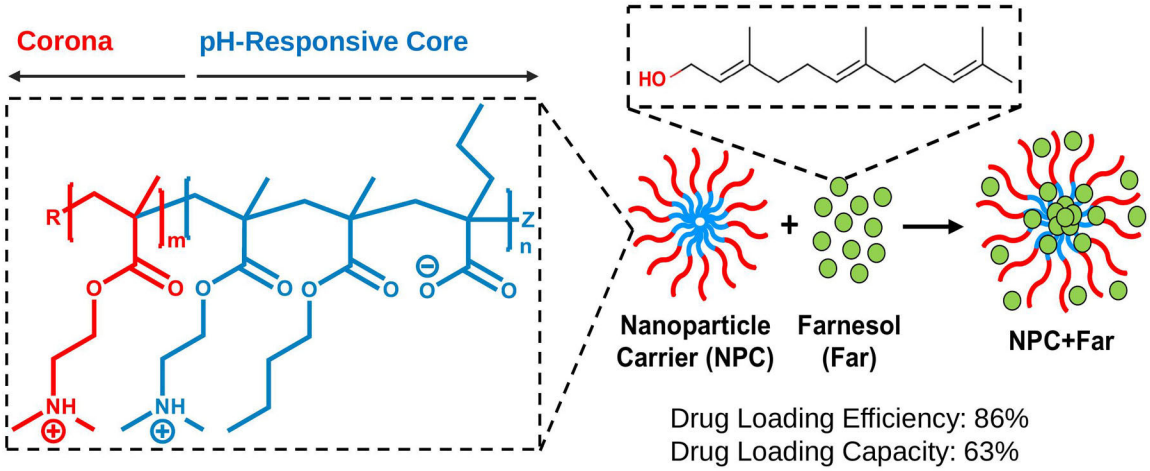

Fig. 1. NPC polymer composition and cartoon illustration of saturated drug loading formulation.
The drug is both loaded into and surrounding NPC used in this study (NP13/4). The red section of the NPC is the cationic, hydrophilic outer corona, and the blue section indicates the hydrophobic, pH-responsive core.

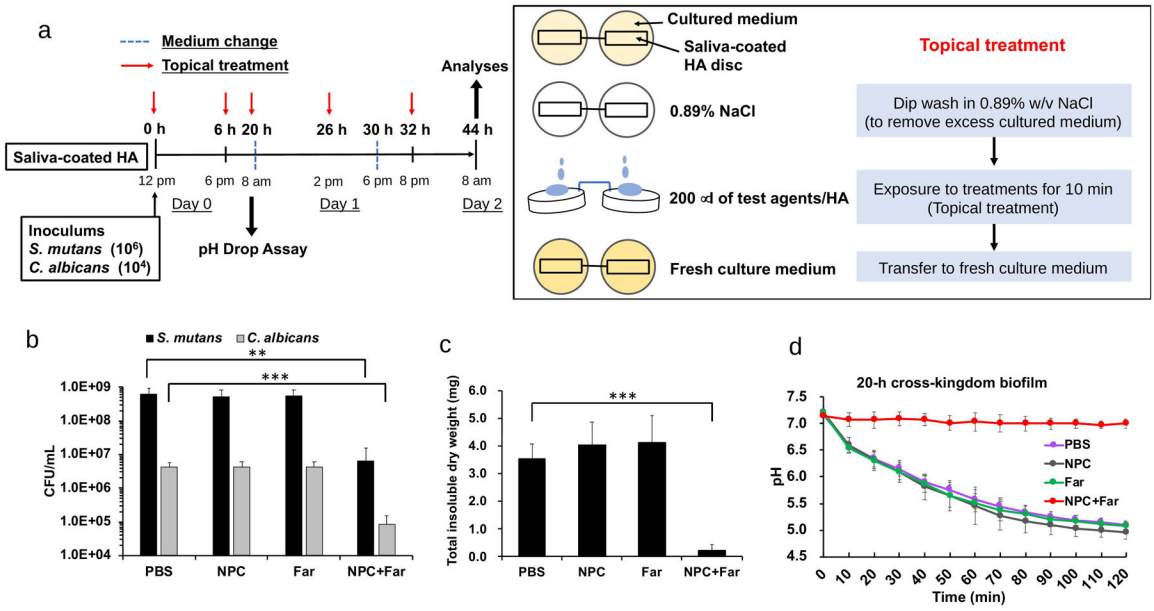

Fig. 2. Antibiofilm performance of NPC+Far on saliva-coated hydroxyapatite (sHA) discs.

(a) Experimental design for topical treatment using sHA biofilm model. (b) Effect of NPC+Far on cell viability, (c) total biomass (insoluble dry weight), and (d) glycolytic activity (pH drop) of the cross-kingdom biofilms.

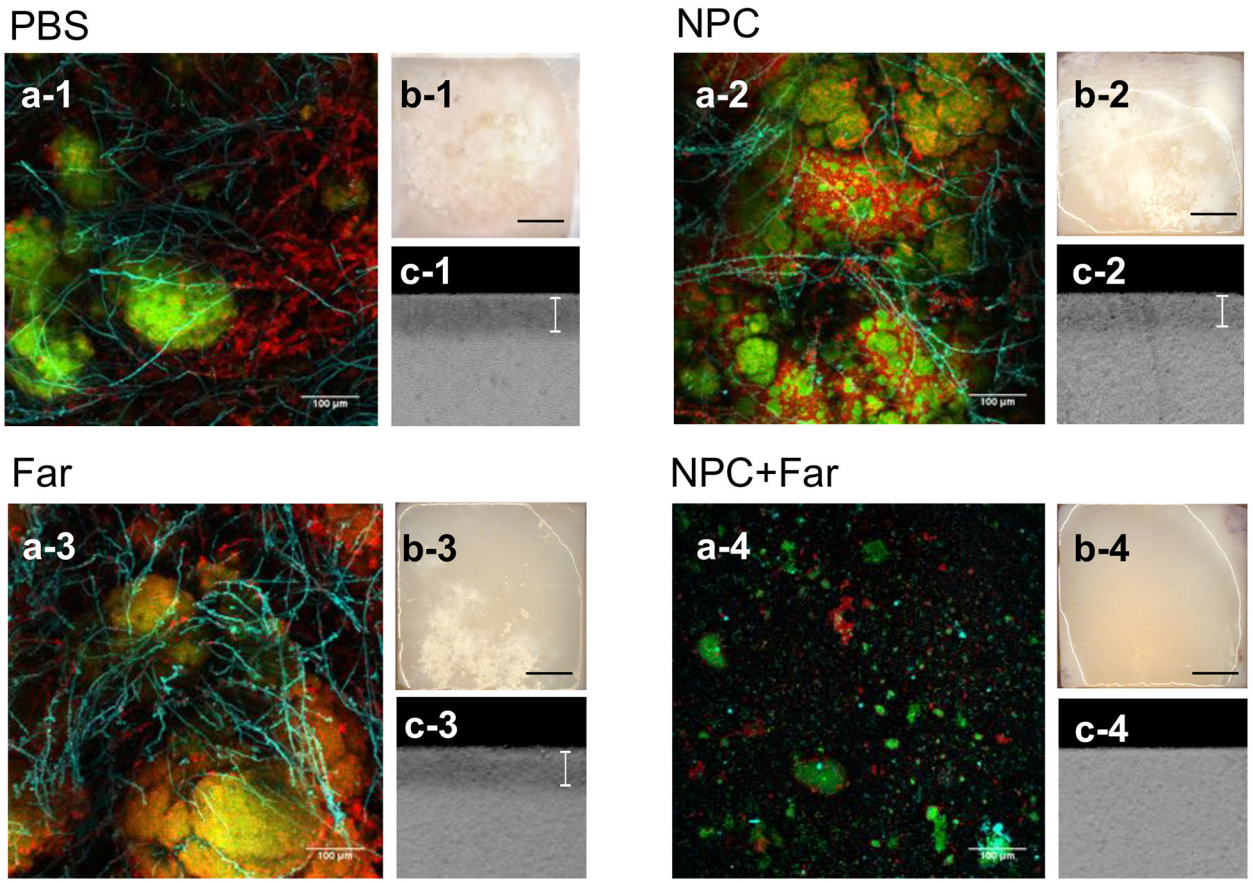

Fig. 3. Antibiofilm performance of NPC+Far on saliva-coated human tooth enamel (sHT) slabs.
(a-1 to a-4) Confocal imaging of the biofilm morphology treated with vehicle, NPC, Far, and NPC+Far, respectively. The bacterial cells are labeled with SYTO 9 (green), the EPS matrix is labeled with Alexa Fluor 647 dextran (red), while *C. albicans* cells are labeled with ConA-tetramethylrhodamine (blue) (Scale bar: 100 μm). (b-1 to b-4) Enamel surface appearance (Scale bar: 1 mm) and (c-1 to c-4) lesion depth of enamel surfaces after treatment with vehicle, NPC, Far, and NPC+Far, respectively. White vertical indicators show the depth of subsurface demineralization.

Table 1.

Polymer and NPC characteristics[Δ]

Polymer								NPC	
Corona block		Core block			Diblock copolymer				
Block 1 M_n (KDa)[1]	Block 2 M_n (KDa)[1]	%DMAEMA[2]	%BMA[2]	%PAA[2]	Overall M_n (KDa)[1]	PDI[1]	CCR[1]	Size (nm)[3]	Charge (ζ, mV)[4]
12.7	3.5	37	57	6	16.2	1.06	3.6	18.6 ± 4.6	+19.7 ± 4.2

Δ As characterized by [1]gel permeation chromatography, [2]nuclear magnetic resonance, [3]dynamic light scattering, and [4]electrophoretic light scattering.

Abbreviations: PDI, polydispersity index (M_W/M_n); CCR, corona-to-core molecular weight ratio; ζ, zeta potential.

Table 2.

Effect of NPC+Far on subsurface demineralization of sHT slabs directly beneath the cross-kingdom biofilms.

Treatment group	Lesion depth (μm)	Mineral loss (vol%.μm)
PBS	26.2 ± 18.9	640 ± 412
NPC	35.3 ± 17.8	790 ± 480
Far	43.7 ± 22.3	893 ± 502
NPC+Far	5.5 ± 3.4 *	98 ± 77 *

The data (mean ± s.d.) is from four independent duplicate experiments (n = 6 to 8). The quantitative data were subjected to Kruskal-Wallis with Dunn's multiple comparison test (* $p < 0.05$, *versus* PBS).